IOSR Journal of Applied Physics (IOSR-JAP)
e-ISSN: 2278-4861.Volume 11, Issue 6 Ser. I (Nov. – Dec. 2019), PP 41-52
www.iosrjournals.org

Crystal, electronic, magnetic and optical structures of cubic double perovskites Ba_2MWO_6 (M = Ni, Zn)

M. Musa Saad H.-E.[1], SalahEldinAshamalla Yousif[2]
[1]*Department of Physics, College of Science and Arts in Muthnib, Qassim University, Muthnib 51931, KSA.*
[2]*Department of Physics, Faculty of Science and Arts in Baljurashi, Albaha University, Baljurashi1998, KSA.*
Corresponding Author: M. Musa Saad H.-E

Abstract: *Based on density functional theory (DFT), the crystal, electronic, magnetic and optical structures of two tungstate double-perovskite oxidesBa_2MWO_6 (M = Ni, Zn) have been explored by employing the local spin density (LSDA) and generalized gradient (GGA) approximations. Two Ba_2MWO_6compounds crystallize in a cubic structure (space group $Fm\bar{3}m$) with 1:1 rock-salt arrangement. Total and partial density of states (DOS) show that Ba_2MWO_6 are semiconductors with energy-gaps in two spins channels. The magnetic calculations reveal that Ba_2MWO_6 behave as antiferromagnetic materials arises from the long-range exchange coupling M^{2+}-$3d^n{}_{\uparrow}$–O^{2-}-$2p^6$–W^{6+}-$5d^0{}_{\downarrow}$. Also, the real and imaginary parts, optical conductivity and electron energy-loss function have been calculated, analyzed and compared with the DOSs results.*

Keywords: Double perovskites; Antiferromagnetic; Optical structures; DFT; LSDA (GGA).

Date of Submission: 13-11-2019 Date of Acceptance: 27-11-2019

I. Introduction

Research on double-perovskite oxides has increased over the last 60 years due to their remarkable properties. Transition-metal double-perovskite oxides, which belong to a large family of magnetic materials, have attracted special attention in many applied and fundamental research in solid-state physics, solid-state chemistry and materials science due to their striking physical and chemical properties. Different charming properties have been observed in these materials, such as room-temperature (RT) colossal magnetoresistance (CMR) in Sr_2MMoO_6 (M = Cr, Fe) [1,2], tunnel magnetoresistance (TMR) in Sr_2FeMoO_6 [3], half-metallic (HM) nature in Sr_2FeMO_6 (M = Mo, Re) and Sr_2CrMO_6 (M = Mo, W) [2,4,5], magnetoelectric in Sr_2CoMoO_6 [6], HM antiferromagnetic (AF) in Sr_2OsMoO_6 and Ba_2FeWO_6 [7,8]. Ordered double perovskites crystallize in the general chemical formula $A_2MM'O_6$, where A, M and M' atoms are arranged on octahedral sites according to the rock-salt type. By substituting the different cations on A, M and/or M' sites by other alkaline-earth metals, transition-metals or any suitable metals, very different crystal, electronic, magnetic and optical structures can be obtained. Therefore, the study of the relationship between these substitutions and the obtained properties has become a hot topic in current research.

Tungstate double-perovskite oxidesA_2MWO_6, with (A = Ca^{2+}, Sr^{2+} and Ba^{2+}) and (M = 3d transition-metal), have been investigated by many researchers. For example, Azad et al. synthesized Ba_2MnWO_6 (A = Ba^{2+}, M = Mn^{2+} and M' = W^{6+}) with a cubic structure and studied its AF properties [9], and Yoshiei et al. investigated the cubic structure and AF ordering of Cu^{2+}–W^{6+} in Ba_2CuWO_6 [10]. Recently, Lopez et al. explored the effective magnetic moments of AF Co^{2+}–W^{6+} system in $A_2Co^{2+}W^{6+}O_6$ within three different crystal structures; A = Ca^{2+} (monoclinic), A = Sr^{2+} (tetragonal) and A = Ba^{2+} (cubic) [11]. Likewise, the physical properties of Ba_2MWO_6, with Ni^{2+}–W^{6+} or Zn^{2+}–W^{6+}, have been characterized by different experimental techniques [12,13], as well they have been theoretically investigated via density functional theory (DFT) calculations [14]. The conclusions of these studies showed that the tungstates Ba_2MWO_6 possess many potential applications, such as can be used in temperature sensors and microwave dielectrics or used as host materials in luminescence applications [9-14].

Motivated by the above mentioned and interesting properties of tungstates A_2MWO_6, especially their inert compounds that containing Ni^{2+} and Zn^{2+}, the crystal, electronic, magnetic and optical structures of two related double perovskites with common formula Ba_2MWO_6 (M = Ni, Zn) have been explored in this study. To the best of our knowledge, there are a few theoretical studies on these compounds in the literature. So, this is the first time to investigate the structures of Ba_2MWO_6 (M = Ni, Zn) by using the first-principles DFT, within the local spin density approximation (LSDA), generalized gradient approximation (GGA) and their correlated methods (LSDA+U and GGA+U). Where, the crystal structures information, ground states, band-gaps, total and partial densities of states, magnetic structures, and optical constants are calculated and discussed in detail. The

present results showed that these two compounds crystallize in cubic structure (space group $Fm\bar{3}m$), and possess an AF with a semiconducting nature.

II. Material And Computational Methods

DFT calculations within the LSDA (Barth-Hedin type) [15] and GGA (Perdew-Wang 91 type) [16] have been utilized to explore the crystal, electronic, magnetic and optical structures of Ba_2MWO_6 (M = Ni, Zn). Furthermore, the calculations have been carried out within the exchange-correlation functional methods (LSDA+U; GGA+U) to take into account the correlation effect beyond LSDA and GGA [15,16]. In LSDA+U and GGA+U calculations, appropriate onsite Coulomb U and exchange J parameters were chosen from a reasonable range that often exploits for 3d-5d states in double perovskites, U_{3d} = 3.0 eV– 6.0 eV and U_{5d} = 1.0 eV– 2.0 eV [8,17-19]. Here for Ba_2MWO_6, parameters U_M = 5.0 eV, U_W = 1.0 eV and $J_M = J_W$ = 0.89 eV are utilized [17,19]. Spin-orbital coupling (SOC) has been included in all calculations. The DFT calculations were performed using the full potential linear muffin-tin orbital (FP-LMTO) implemented in LMTART software [20,21]. FP-LMTO relies on the self-consistent (SCF) potential borrowed from the LMTO calculations. For SCF calculation with plane wave (PLW) basis, the number of *k*-points was chosen to be 120 with 6×6×6 Brillouin-zone k-point grid, and have been checked for convergence. The criterion that relating the PLW and angular-momentum cutoff ($L_{Max} = R_{Max} \times K_{Max}$) was taken to be 6.0, where R_{Max} and K_{Max} are the maximum muffin-tin sphere (MTS) radius and PLW cutoff, respectively. The MTS radii were chosen from the charge neutrality condition inside the spheres; so that the total formula-unit volumes close to the experimental ones, see Table 1.

Table 1. Atomic radii of the MTSs and ionic radii R that set in FP-LMTO calculations

compound		Ba^{2+}	M^{2+}	W^{6+}	O^{2-}
Ba_2NiWO_6	MTS (a. u.)	3.7460	2.2750	2.1830	1.5170
	R (Å)	1.61	0.69	0.60	1.41
Ba_2ZnWO_6	MTS (a. u.)	3.7460	2.2750	2.1830	1.5170
	R (Å)	1.61	0.74	0.60	1.41

III. Result And Discussion

3.1. Crystal structuresof Ba_2MWO_6

After full structural-optimization calculations are completed, the crystals of Ba_2MWO_6 (M = Ni, Zn) obviously showed an ideal 1:1 cation ordering due to the large difference in size and charge between M^{2+} and W^{6+} cations. As a result, the crystal structures of these two compounds stabilized in face-centered cubic with space group $Fm\bar{3}m$ (no. 225). Detail crystal structures data at RT, the calculated tolerance factor (T_F), lattice constants (a, b, c; α, β, γ), formula unit volume (V), and oxygen positions O (*x*) are shown in Table 2 and compared with the available experimental and theoretical results. T_F is calculated via ($T_F = (R_{Ba} + R_O)/\sqrt{2}((R_M + R_W)/2 + R_O)$) by using the ionic radii of Ba^{2+} in a 12-coordinate polyhedral system; and M^{2+}, W^{6+}, and O^{2-} in a 6-coordinate octahedral system [22], as they were summarized in Table 1. As shown in Table 2, the crystals of Ba_2MWO_6 are in stable state and adopt cubic structures with T_F = 1.0427 (M = Ni) and T_F = 1.03351 (M = Zn), in the usual range of similar cubic double perovskites (T_F = 0.99–1.05) [8,23]. Lattice constants are approximately equal to the ideal value ($a = b = c = 2a_0$; a_0 = 4 Å) with a slight deviation from experimental results, 0.0831 Å and 0.0813 Å for M = Ni and Zn, respectively. Thecoordinates O (*x*)differ by a small amount of 0.17 and is mostly depend on the sort of atom that occupies M-site in Ba_2MWO_6. Also, it is seen that the parameters *a*, V and O (*x*) linearly increase in the sequence of M = Ni^{2+} and Zn^{2+}. The DFT results are in a good agreement with the X-ray diffraction (XRD) [24,28] and neutron powder diffraction (NPD) [24,25,26,28].

Table 2. Crystal structures data of Ba_2MWO_6 (M = Ni, Zn) at RT (298 K), compared with the XRD and NPD experiments and other calculations results.

Method	Symmetry	T_F	a = b = c (Å)	α = β = γ (°)	V (Å^3)	O (x)
Ba_2NiWO_6						
DFT	$Fm\bar{3}m$	1.0427	8.0592	90.000	511.419	0.2603
Exp. XRD [24]	$Fm\bar{3}m$		8.0701		525.617	0.2346
Exp. NPD [24-26]	$Fm\bar{3}m$	1.0200	8.0807	90.000	527.65	0.2332
Cal. [27]	$Fm\bar{3}m$		8.0640	90.000		0.2590
Ba_2ZnWO_6						

DFT	$Fm\bar{3}m$	1.0351	8.0950	90.000	522.63	0.2620
Exp. XRD [28]	$Fm\bar{3}m$		8.1363		538.61	0.2376
Exp. NPD [28]	$Fm\bar{3}m$	1.0080	8.1210	90.000	535.59	0.2370
Cal. [14,28]	$Fm\bar{3}m$		8.1100	90.000		0.2610

Table 3 shows the atomic multiplicity, Wyckoff symbol, site-symmetry, coordinates (x, y, z) and occupation numbers for the cubic Ba_2MWO_6 (M = Ni, Zn) at RT. Also, the main bond-sizes of Ba–O, M–O and W–O, and bond-angles of M–O and M–O–W are calculated at RT and summarized in Table 4. As shown in Fig. 1, the crystal structure of Ba_2MWO_6 describes the face-centered cubic arrangement of M and W atoms in a rock-salt (Na^+Cl^-) type, where, M^{2+} located at 4a (0,0,0) and W^{6+} at 4b (½,½,½) to form a face-centered cubic lattice with a half displacement of lattice constant. The O^{2-} atoms located at 24e (*x*,0,0) near the center ($x \approx ¼$) of nearest-neighboring M^{2+} and W^{6+} atoms (M^{2+}–O^{2-}–W^{6+}) with equal bond-sizes, M^{2+}–$O^{2-} \approx O^{2-}$–$W^{6+} \approx$ 2 Å. Accordingly, only six O^{2-} surround the central M^{2+} and W^{6+} atoms that forming two different MO_6 and WO_6octahedra. Whereas the Ba^{2+} atoms located at 8c (¼,¼,¼) in the middle of the hollow space produced by the corner-sharing octahedra that linking in a straight angle (MO_6–WO_6 = 180º).

Table 3. Atomic multiplicity, Wyckoff, site-symmetry, coordinates and occupation number for cubic crystal structure ($Fm\bar{3}m$) of Ba_2MWO_6 (M = Ni, Zn) at RT.

Atom	Multiplicity	Wyckoff	Site-symmetry	*x*	*y*	*z*	Occupation
Ba_2NiWO_6							
Ba^{2+}	8	C	-43m	0.2500	0.2500	0.2500	1.000
Ni^{2+}	4	A	m-3m	0.0000	0.0000	0.0000	1.000
W^{6+}	4	B	m-3m	0.5000	0.5000	0.5000	1.000
O^{2-}	24	E	4m.m	0.2603	0.0000	0.0000	6.000
Ba_2ZnWO_6							
Ba^{2+}	8	C	-43m	0.2500	0.2500	0.2500	1.000
Zn^{2+}	4	A	m-3m	0.0000	0.0000	0.0000	1.000
W^{6+}	4	B	m-3m	0.5000	0.5000	0.5000	1.000
O^{2-}	24	E	4m.m	0.2620	0.0000	0.0000	6.000

Table 4. Main bond-sizes and bond-angles for cubic crystal structure ($Fm\bar{3}m$) of Ba_2MWO_6 (M = Ni, Zn) at RT, compared with the available XRD and NPD experimental results.

Bond-size/ Bond-angle	DFT	XRD [24-28]	NPD [24-28]
Ba_2NiWO_6			
Ba (8c)–O (24e) ×12 (Å)	2.8502	2.8523	-
Ni (4a)–O (24e) ×6 (Å)	2.0815	2.1229	-
W (4b)–O (24e) ×6 (Å)	1.9206	1.9167	-
Ni (4a)–O (24e) (°)	90.000	90.000	-
Ni (4a)–O (24e)–W (4b) (°)	180.00	180.00	-
Ba_2ZnWO_6			
Ba (8c)–O (24e) ×12 (Å)	2.8653	2.8783	2.8732
Zn (4a)–O (24e) ×6 (Å)	2.1105	2.1353	2.1362
W (4b)–O (24e) ×6 (Å)	1.92900	1.9333	1.9245
Zn (4a)–O (24e) (°)	90.000	90.000	90.000
Zn (4a)–O (24e)–W (4b) (°)	180.00	180.00	180.00

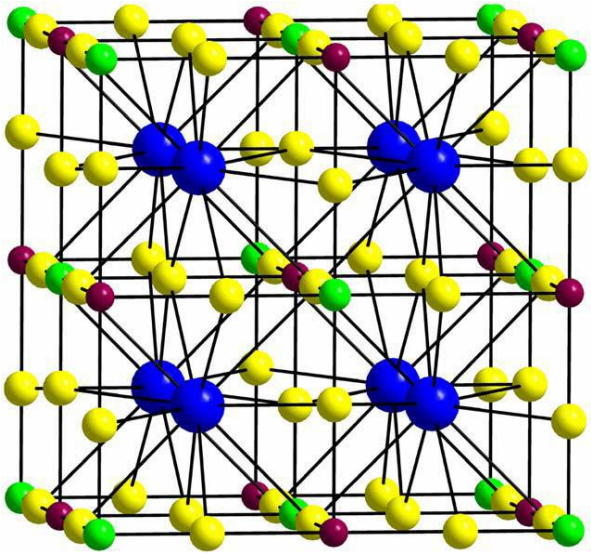

Fig. 1. The face-centered cubic arrangement of atoms in crystal structure of Ba_2MWO_6 (M = Ni, Co); Ba (blue), M (brown red), W (green) and O (yellow).

3.2. DFT electronic structuresof Ba_2MWO_6

3.2.1. Total density of states

The DFT total density of states (TDOS) per formula unit of Ba_2MWO_6 (M = Ni, Zn) have been calculated using LSDA, LSDA+U, GGA and GGA+U methods and shown in Fig. 2, U_M = 0.0 eV and U_W = 0.0 eV are set in LSDA and GGA, whereas U_M = 5.0 eV and U_W = 1.0 eV are utilized in LSDA+U and GGA+U. The TDOS close to the Fermi level (E_F = 0.0 eV) show that the Ba_2MWO_6 compounds are semiconductors with energy-gaps (E_g) in spin-up and spin-down channels within all methods. E_F falls in the gap between the valence and conduction states, and the values of E_g in the spin-up and spin-down channels ($TDOS_\uparrow$ and $TDOS_\downarrow$) of Ba_2MWO_6 (M = Ni, Zn) are calculated by these four methods and summarized in Table 5. The main remark from Fig. 2, that the LSDA (GGA) and LSDA+U (GGA+U) methods yield similar shape of TDOS in each compound of Ba_2MWO_6 with small differences in peaks. However, the TDOS based on LSDA+U and GGA+U show large E_g than that obtained using LSDA and GGA. In M = Ni compound, the valence states appear as high peaks between –8.0 eV and E_F, and the conduction states emerge as two separated low peaks between E_F and +8.0 eV. Whereas in M = Zn compound, high symmetrical peaks appear in the valence states between –7.5 eV and E_F, and two low-peaks emerge in the conduction states between E_F and +10.0 eV. In M = Ni, the $E_{g\uparrow}$ and $E_{g\downarrow}$ expand from 0.0 eV to +1.16 eV ($E_{g\uparrow}$ = 1.16 eV) and from –0.20 eV to +0.48 eV ($E_{g\downarrow}$ = 0.68 eV) within LSDA; from 0.0 eV to +1.18 eV ($E_{g\uparrow}$ = 1.18 eV) and from –0.18 eV to +0.50 eV ($E_{g\downarrow}$ = 0.68 eV) within GGA. Then they enlarge; from –0.08 eV to +2.00 eV ($E_{g\uparrow}$ = 2.08 eV) and from 0.0 eV to +2.18 eV ($E_{g\downarrow}$ = 2.18 eV) within LSDA+U; and from –0.08 eV to +1.96 eV ($E_{g\uparrow}$ = 2.04 eV) and from 0.0 eV to +2.18 eV ($E_{g\downarrow}$ = 2.18 eV) within GGA+U. On the contrary, in M = Zn case, the $E_{g\uparrow}$ and $E_{g\downarrow}$ are equally expanded in TDOS from 0.0 eV to +2.12 eV ($E_{g\uparrow}$ = 1.12 eV) and ($E_{g\downarrow}$ = 2.12 eV) within LSDA and GGA; and from 0.0 eV to +2.35 eV ($E_{g\uparrow}$ = 2.35 eV) and ($E_{g\downarrow}$ = 0.68 eV) within LSDA+U and GGA+U. From these results, it can be concluded that the increase of $E_{g\uparrow}$ and $E_{g\downarrow}$ exposes the effect of both U energy (LSDA+U and GGA+U) and M-site substitution (M = Ni^{2+}-$3d^8$ and Zn^{2+}-$3d^{10}$). U energy has the largest effect; it opens the $TDOS_\uparrow$ and $TDOS_\downarrow$ around the E_F.

Table 5. Spin-up and spin-down energy gaps in the TDOS channels (Fig. 2) for Ba_2MWO_6 (M = Ni, Zn) calculated by the LSDA, GGA, LSDA+U and GGA+U methods.

Ba_2MWO_6	M = Ni		M = Zn	
Channel	$E_{g\uparrow}$ (eV)	$E_{g\downarrow}$ (eV)	$E_{g\uparrow}$ (eV)	$E_{g\downarrow}$ (eV)
LSDA	1.16	0.68	2.12	2.12
GGA	1.18	0.68	2.12	2.12
LSDA+U	2.08	2.18	2.35	2.35
GGA+U	2.04	2.18	2.35	2.35

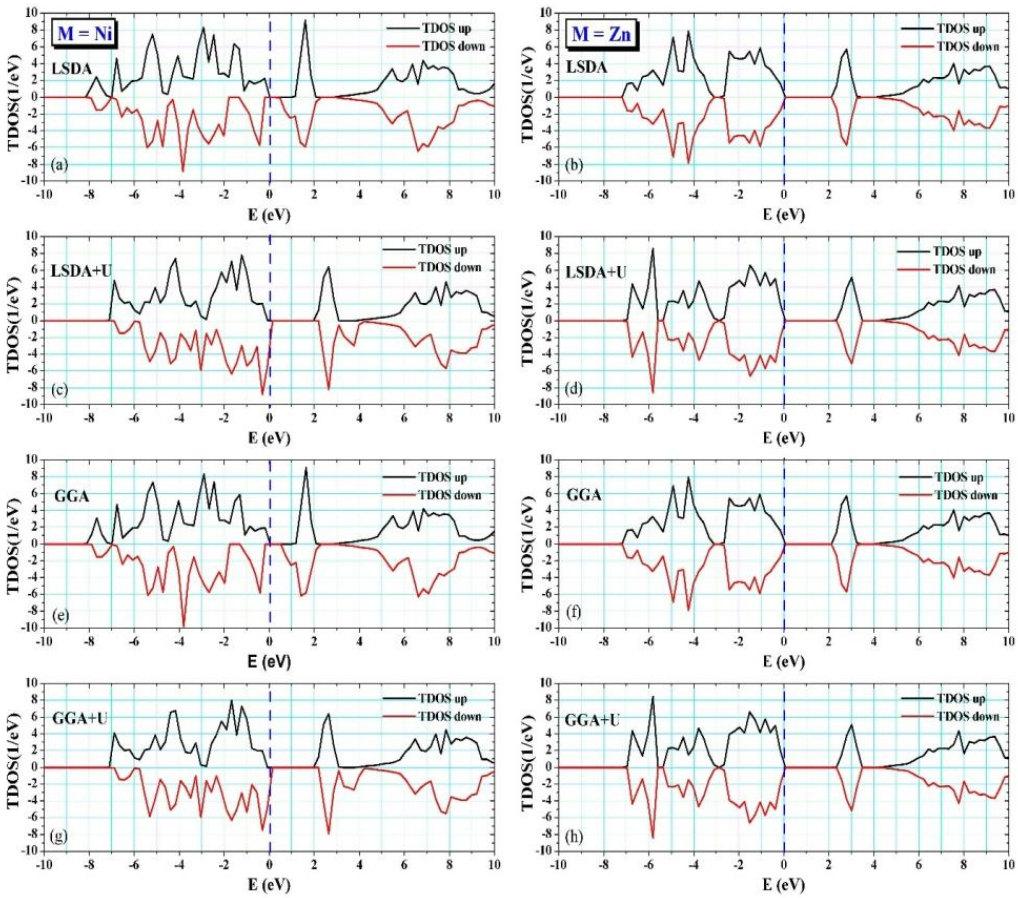

Fig. 2. Spin-up and spin-down total density of states (TDOS up and TDOS down) of Ba_2MWO_6 (M = Ni, Zn) from LSDA (a) and (b), LSDA+U (c) and (d), GGA (e) and (f), and GGA+U (g) and (h) methods. The dashed line represents the Fermi energy (E_F).

3.2.2. Partial density of states

The TDOS and projected partial density of states (PDOS) of M-3d, W-5d, and O-2p for Ba_2MWO_6 (M = Ni, Zn) have been also calculated using LSDA, LSDA+U, GGA and GGA+U methods, plotted and shown in Fig. 3 (M = Ni) and Fig. 4 (M = Zn). First, for Ba_2NiWO_6, there are two distinct peaks with DOS of about 4.0 and 1.0 State/eV in $PDOS_\uparrow$ contributed by Ni-$3d_\uparrow$ states, expand between –2.0 eV and the E_F in the top of the valence band, within LSDA (panel a) and GGA (panel c). Besides, there is a little effect come from the admixture of Ni-$3d_\uparrow$, W-$5d_\uparrow$, and O-$2p_\uparrow$ states between –8.0 eV and –2.0 eV. In $PDOS_\downarrow$, a single sharp peak of Ni-$3d_\downarrow$ (DOS of 4.3 State/eV) appears in the range –1.5 eV to –0.3 eV beyond E_F. Whereas, a sharp peak of W-$5d_\uparrow$ (DOS = 4.8 State/eV) emerges between +1.0 eV and 2.0 eV in bottom of the conduction band, plus, two overlapping spin-down peaks contributed by Ni-$3d_\downarrow$ (DOS = 2.0 State/eV) and W-$5d_\downarrow$ (DOS = 2.5 State/eV) emerge between +0.5 eV and +2.0 eV. In addition, there are small W-$5d_\uparrow$ and W-$5d_\downarrow$ states expand in front of the conduction band, between +3.0 eV and +8.0 eV. In LSDA+U (panel b) and GGA+U (panel d), it can be seen that the valence band of Ba_2NiWO_6 nearly affected by the introducing of U energy; all PDOS of Ni-$3d_\uparrow$ states emerge as splitting peaks between –7.0 eV and E_F with low DOS, except for a single sharp peak of Ni-$3d_\downarrow$ states (DOS = 4.5 State/eV) at the E_F. While the $PDOS_\uparrow$ and $PDOS_\downarrow$ of Ni-3d and W-5d in the conduction band are unaffected by this energy, except two splitting peaks of Ni-$3d_\downarrow$ (DOS = 2.0 State/eV) and W-$5d_\downarrow$ (DOS = 3.5 State/eV) emerge between +2.0 eV and +4.0 eV.

Second, from the DOS of Ba_2ZnWO_6 in Fig. 4 (panels a–c), it is clear that all $TDOS_{\uparrow\downarrow}$ and $PDOS_{\uparrow\downarrow}$ calculated by LSDA, LSDA+U, GGA and GGA+U methods look similar. The main peaks Zn-$3d_{\uparrow\downarrow}$, W-$5d_{\uparrow\downarrow}$, and O-$2p_{\uparrow\downarrow}$ are evenly distributed in the valence and conduction bands. Also, these peaks expand in symmetrical $DOS_\uparrow$ and $DOS_\downarrow$ beyond and in front of E_F because their 3d orbitals are completely filled, Zn-$3d^{10}$. The valence band consists mainly of high symmetrical peaks of Zn-$3d_\uparrow$ and Zn-$3d_\downarrow$, expand between –7.5 eV and –3.5 eV with equal DOS ($DOS_{\uparrow\downarrow}$ = 5.0 State/eV; LSDA and GGA) and ($DOS_{\uparrow\downarrow}$ = 7.0 State/eV; LSDA+U and GGA+U). While the conduction band contains only symmetrical peak ($DOS_{\uparrow\downarrow}$ = 2.5 State/eV) within all methods, contributed by the W-$5d_\uparrow$ and W-$5d_\downarrow$ states in the range +2.5 eV– +3.5 eV. The additional minute contributions of Zn-$3d_{\uparrow\downarrow}$, W-$5d_{\uparrow\downarrow}$, and O-$2p_{\uparrow\downarrow}$ states expand between –3.0 eV and E_F and between +5.0 eV and +9.0 eV.

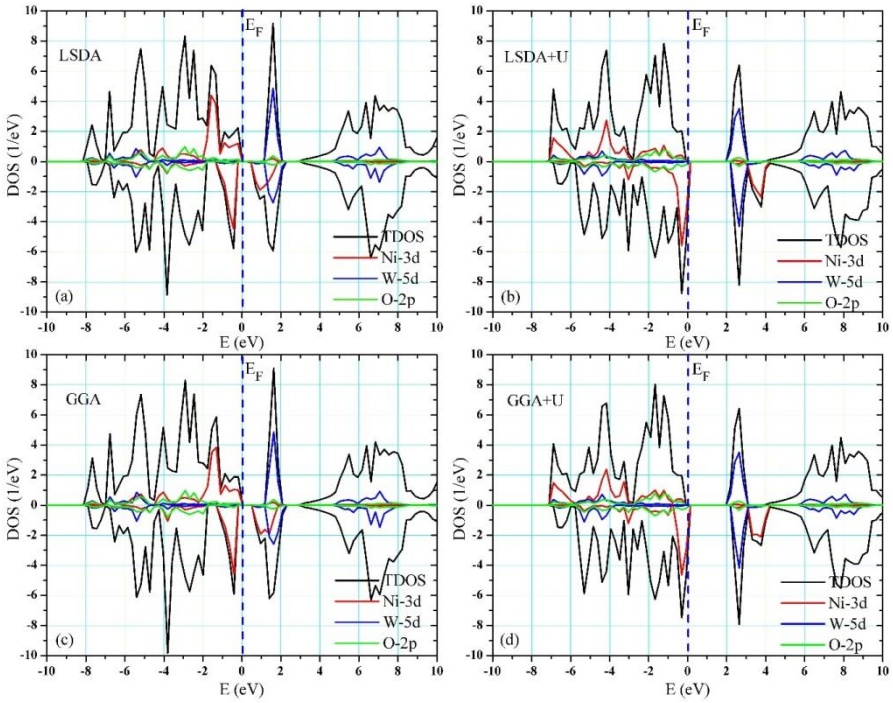

Fig. 3. Spin-up and spin-down TDOS and PDOSs (Ni-3d, W-5d, and O-2p) of Ba_2NiWO_6 within LSDA, LSDA+U, GGA and GGA+U methods. The dashed line represents the Fermi energy (E_F).

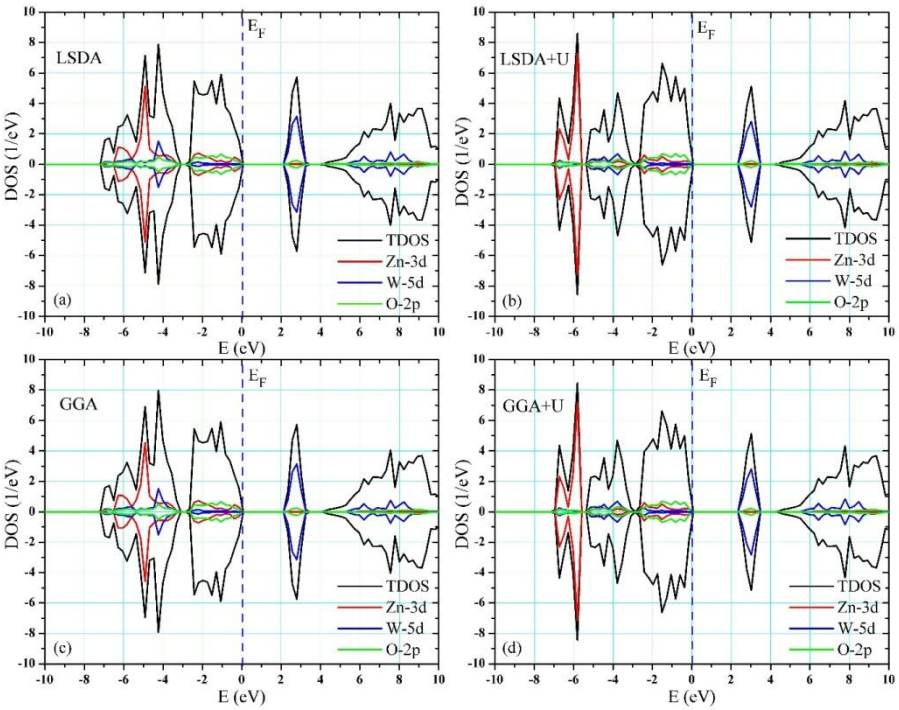

Fig. 4. Spin-up and spin-down TDOS and PDOSs (Zn-3d, W-5d, and O-2p) of Ba_2ZnWO_6 within LSDA, LSDA+U, GGA and GGA+U methods. The dashed line represents the Fermi energy (E_F).

Figs. 5 and 6 represent the spin-up and spin-down PDOSs of M-3d and W-5d orbitals in Ba_2MWO_6 (M = Ni, Zn) calculated using LSDA+U and GGA+U methods. It is clear that there are E_g at E_F in both spin-up and spin-down channels, which produce the semiconducting structure in two compounds. Also, it can be seen that the TDOS is mainly contributed by the M-3d and O-2p states in the range from – 2.0 eV to +2.0 eV through E_F. And beyond this range, W-5d states give a small contribution. Considering the main peaks close to E_F, that the presence of an octahedral crystal field due to the six O-2p atoms surrounding the M-3d and W-5d sites in MO_6

and WO_6octahedra, the five-fold degenerate 3d and 5d orbitals split into triply degenerate t_{2g} (yz, xz, xy) substates with lower energy and doubly degenerate e_g (z^2, x^2-y^2) substates with higher energy. This splitting takes place in both spin-up and spin-down channels. From the PDOS of Ni-3d in Fig. 5, the spin-splitting is about 1.2 eV (LSDA+U) and 1.8 eV (GGA+U), which they force the spin-down substates of 3d-$t_{2g\downarrow}$ (yz, xz, xy) to hop toward E_F at –0.5 eV causing full-occupation states, and spin-up 3d-$t_{2g\uparrow}$ (yz, xz, xy) substates are also fully occupied and lie at –1.5 eV beyond E_F. While, the splitting of Ni-3d (e_g) substates near E_F is 2.1 eV (LSDA+U) and 3.8 eV (GGA+U); the occupied spin-up substates of $e_{g\uparrow}$ (z^2, x^2-y^2) lie at E_F, as the unoccupied spin-down $e_{g\downarrow}$ (z^2, x^2-y^2) hop away from E_F at +1.2 eV and +3.5 eV, respectively. From the PDOS of W-5d in Fig. 5, the splitting is minute due to the empty of W-5d (t_{2g}) and W-5d (e_g) substates; there is a symmetry in spin-up and spin-down of 5d-$t_{2g\uparrow\downarrow}$ (yz, xz, xy) that lie beyond E_F at +1.5 eV (LSDA+U) and +2.5 eV (GGA+U). Conversely, the octahedral crystal field is not materialized in Ba_2ZnWO_6 since it contains completely occupied states in Zn^{2+} ($3d^{10}$) orbitals interact with empty states of W^{6+} ($5d^0$). Therefore, it is seen from Fig. 6 the t_{2g} (yz, xz, xy) and e_g (z^2, x^2-y^2) substates emerge as separated symmetrical peaks lie beyond E_F. The occupied Zn-3d ($t_{2g\uparrow\downarrow}$) substates lie at –5.0 eV (LSDA+U) and +6.0 eV (GGA+U), whereas there is small symmetrical PDOS of 3d-$e_{g\uparrow\downarrow}$ (z^2, x^2-y^2) between –2.5 eV and E_F, which predict a full occupation state in Zn-3d ($e_{g\uparrow\downarrow}$) substates. In two compounds, both spin-up and spin-down of degenerated substates W-5d ($e_{g\uparrow\downarrow}$), that located respectively at about +7.0 eV (LSDA+U) and +8.0 eV (GGA+U), are unoccupied.

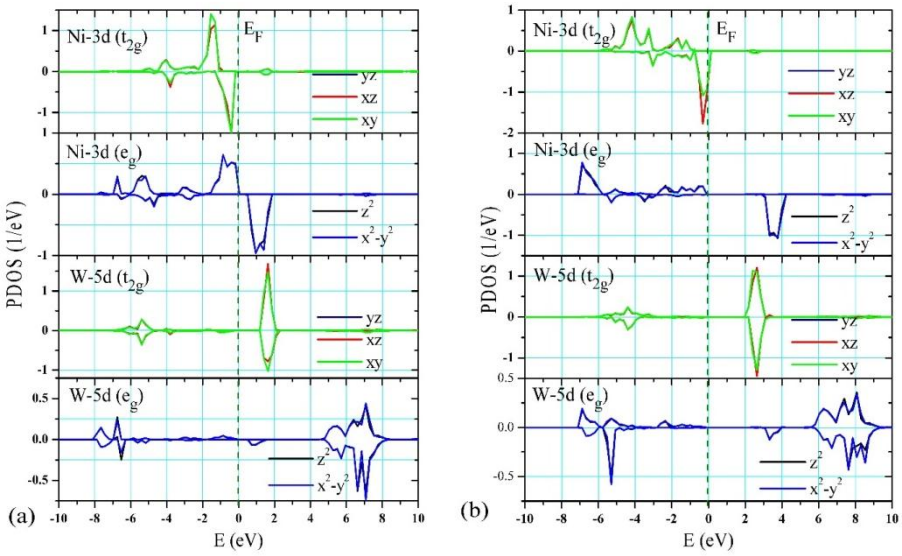

Fig. 5. Spin-up and spin-down PDOSs of Ni-3d ($t_{2g}e_g$) and W-5d ($t_{2g}e_g$) in Ba_2NiWO_6 within LSDA+U and GGA+U methods. The dashed line represents the Fermi energy (E_F).

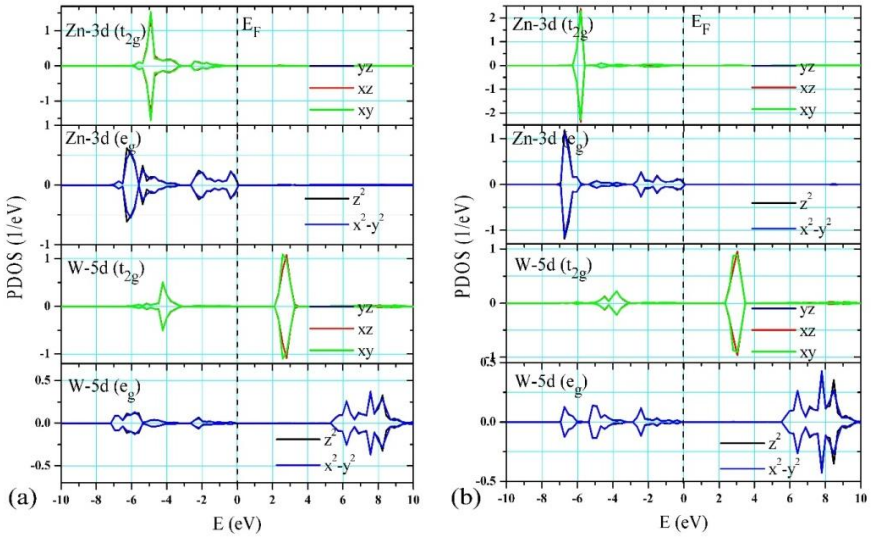

Fig. 6. Spin-up and spin-down PDOSs of Zn-3d ($t_{2g}e_g$) and W-5d ($t_{2g}e_g$) in Ba_2ZnWO_6 within LSDA+U and GGA+U methods. The dashed line represents the Fermi energy (E_F).

3.2.3. Charge density

In order to distinguish the contribution of each atom on the electronic structure of Ba_2MWO_6 (M = Ni, Zn), the spin-up and spin-down partial occupations of Ba^{2+}-6s, M^{2+}-3d, W^{6+}-5d, and O^{2-}-2p orbitals are calculated within LSDA, LSDA+U, GGA and GGA+U, and listed in Table 6. It is known that the interaction between M^{2+}-3d and W^{6+}-5d, and their surrounding O^{2-}-2p ions has some degrees of covalency that result from the sharing of valence electrons via the AF long-range pdd-π superexchange interaction M^{2+}-3d–O^{2-}-2p_π–W^{6+}-5d. Since the two compounds of Ba_2MWO_6 crystallize in a cubic symmetry, the M–O–W bond is 180°, with M being for Ni-$3d^8$ and Zn-$3d^{10}$ ions with full-filled spin-up and spin-down of t_{2g} states; and half-filled and full-filled spin-up and spin-down of e_g states, respectively. The intermediate O^{2-}-$2p^6$ ions share their spin-down electrons with the M-3d-e_g ions via M–O bonds, which they would hop to the empty orbitals in M-3d-e_g , and this forces the hopping electrons to align in spin-down direction $e_g^1{}_\downarrow$ and $e_g^2{}_\downarrow$ in Ni^{2+}-$3d^8$ and Zn^{2+}-$3d^{10}$, respectively. This leaves the remaining spin-down electrons on O^{2-}-$2p^6$ to be shared with the W^{6+}-$5d^0$ (t_{2g}^0 e_g^0) via O–W bonds, thereby inducing the t_{2g} electrons to align in spin-up direction, $t_{2g\uparrow}$. Thus, the superexchange interaction M^{2+}-3d–O^{2-}-2p_π–W^{6+}-5d, between two neighboring ions in the case of cubic Ba_2MWO_6, leads to an AF coupling through the indirect hopping of electrons between these orbitals. As a result, the amount of charge on M-3d and W-5d ions indicates that both of them change their valance states relative to the number of electrons that occupying the e_g and t_{2g} orbitals in 3d and 5d, respectively.

Table 6. Spin-up and spin-down partial occupations in Ba_2MWO_6 (M = Ni, Zn).

Orbital	Ba-6s		M-3d		W-5d		O-2p	
	$6s_\uparrow$	$6s_\downarrow$	$3d_\uparrow$	$3d_\downarrow$	$5d_\uparrow$	$5d_\downarrow$	$2p_\uparrow$	$2p_\downarrow$
Ba_2NiWO_6								
LSDA	0.1406	0.1415	4.8580	3.2895	1.2946	1.2844	1.8001	1.7447
LSDA+U	0.1414	0.1419	4.9126	3.1840	1.2809	1.2727	1.7927	1.7595
GGA	0.1408	0.1417	4.8596	3.2861	1.2930	1.2852	1.7999	1.7445
GGA+U	0.1416	0.1421	4.9132	3.1815	1.2803	1.2725	1.7924	1.7594
Ba_2ZnWO_6								
LSDA	0.1424	0.1424	4.9610	4.9610	1.2736	1.2736	1.7769	1.7769
LSDA+U	0.1425	0.1425	4.9680	4.9680	1.2713	1.2714	1.7770	1.7770
GGA	0.1426	0.1426	4.9610	4.9610	1.2733	1.2733	1.7766	1.7766
GGA+U	0.1427	0.1427	4.9680	4.9680	1.2713	1.2708	1.7766	1.7767

For the semiconducting nature in Ba_2MWO_6, it can see that from Table 6 the spin-up and spin-down occupations of 3d orbitals are equal in all calculations; ~$4.9e_\uparrow$ and ~$3.0e_\downarrow$ for Ni-3d ions, and ~$4.9e_\uparrow$ and ~$4.9e_\downarrow$ for Zn-3d ions, which demonstrates the accurate ionic states Ni^{2+}-$3d^8$ and Zn^{2+}-$3d^{10}$, respectively. W-5d orbitals are equally occupied by symmetrical electrons, ~$1.3e_\uparrow$ and ~$1.3e_\downarrow$, which reveals the zero state in W^{6+}-$5d^0$ ions. The occupations ~$1.8e_\uparrow$ and ~$1.8e_\downarrow$ for O^{2-}-$2p^6$ expose the sharing of two electrons between M-3d and W-5d via O-2p orbitals. Besides, the Ba^{2+}-6s orbitals have a small amount of charge in ionic bonds relative to their oxidation state +2. Therefore, the most effective charges on Ni^{2+}-$3d^8$, Zn^{2+}-$3d^{10}$, and W^{6+}-$5d^0$ indicate a considerable amount of covalence charge exists in the interaction bonds of M-3d–O-2p and W-5d–O-2p.

3.3. DFT magnetic structuresof Ba_2MWO_6

The magnetic structures of Ba_2MWO_6 (M = Ni, Zn) are addressed by calculating the partial and total spin magnetic moments within LSDA, LSDA+U, GGA and GGA+U. Table 7 displays the electronic configuration of atoms, valence state and ionic spin configuration for the ground states of Ba_2MWO_6.Besides**,** the partial spin magnetic moments and total spin magnetic moment per formula unit are calculated and summarized in Table 8. The magnetic results indicate that the M^{2+}-3d ions have high-spin configuration, Ni^{2+}-$3d^8$; $t_{2g}^3{}_\uparrow$ $t_{2g}^3{}_\downarrow$ $e_g^2{}_\uparrow$ $e_g^0{}_\downarrow$, (S = 1 μ_B/f.u.) and Zn^{2+}-$3d^{10}$; $t_{2g}^3{}_\uparrow$ $t_{2g}^3{}_\downarrow$ $e_g^2{}_\uparrow$ $e_g^2{}_\downarrow$, (S = 0 μ_B/f.u.), whereas the W^{6+} ions have non-magnetic spin configuration W^{6+}-$5d^0$; $t_{2g}^0{}_\uparrow$ $t_{2g}^0{}_\downarrow$ $e_g^0{}_\uparrow$ $e_g^0{}_\downarrow$, (S = 0 μ_B/f.u.). Accordingly, there is a major difference between two compounds, the formula unit of Ba_2NiWO_6 includes eight electrons in its partially filled Ni-3d orbitals that interacting with empty W-5d orbitals ($5d^8$–$5d^0$), while the fully filled Zn-3d orbitals interact also with the empty W-5d orbitals ($3d^{10}$–$5d^0$). These interactions prove the difference in electronic and magnetic structures between two compounds. The values of the total spin magnetic moments for Ba_2MWO_6 (M = Ni, Zn) are predicted to be 1.0 μ_B/f.u. and 0.0 μ_B/f.u., respectively, in a good agreement with the experimental results [23,24]. For Ba_2NiWO_6, the main contribution to the total spin magnetic moment comes from Ni^{2+}-$3d^8$ and O^{2-}-2p ions, while Ba^{2+}-6s and W^{6+}-$5d^0$ give very small contributions. While, all Ba^{2+}-6s, Zn^{2+}-$3d^{10}$, W^{6+}-$5d^0$, and O^{2-}-2p ions contribute very little to total spin magnetic-moment of Ba_2ZnWO_6, roughly equal to zero. Besides the effect of M-site substitution, the calculations results of the partial spin magnetic moments when using LSDA+U and GGA+U methods verified the major effect of the exchange-correlation energy U. There is a small increase in spin magnetic moments of Ni^{2+} and Zn^{2+} ions, whereas for W^{6+} ions, they decrease slightly compared to their calculated values using LSDA and GGA methods.

Table 7. Atomic and ionic configurations, valence states and ionic spin values for the atoms in the ground state of Ba_2MWO_6 (M = Ni, Zn).

Atom	Atomic Configuration	Valence state	Ionic Configuration	Spin S
Ba	[Xe] $6s^2$	2+	Ba^{2+}-$6s^0$	0
Ni	[Ar] $3d^8$ $4s^2$	2+	Ni^{2+}-$3d^8$; $t_{2g}^3\uparrow$ $t_{2g}^3\downarrow$ $e_g^2\uparrow$ $e_g^0\downarrow$	1
Zn	[Ar] $3d^{10}$ $4s^2$	2+	Zn^{2+}-$3d^{10}$; $t_{2g}^3\uparrow$ $t_{2g}^3\downarrow$ $e_g^2\uparrow$ $e_g^2\downarrow$	0
W	[Xe] $4F^{14}$ $5d^4$ $6s^2$	6+	W^{6+}-$5d^0$; $t_{2g}^0\uparrow$ $t_{2g}^0\downarrow$ $e_g^0\uparrow$ $e_g^0\downarrow$	0
O	[He] $2s^2$ $2p^4$	2–	O^{2-}-$2s^0$ $2p^0$	0

Table 8. Partial and total spin magnetic moments (μ_B) in Ba_2MWO_6 (M = Ni, Zn)

Orbital	Ba-6s	M-3d	W-5d	O-2p	Total
Ba_2NiWO_6					
LSDA	–0.0120	1.5753	0.0301	0.0645	1.0
LSDA+U	–0.0091	1.7001	0.0214	0.0401	1.0
GGA	–0.0127	1.5834	0.0275	0.0645	1.0
GGA+U	–0.0095	1.7434	0.0209	0.0399	1.0
Ba_2ZnWO_6					
LSDA	0.9E–6	0.14E–6	0.55E–5	–0.14E–6	0.0
LSDA+U	0.53E–5	0.34E–6	0.91E–4	–0.18E–4	0.0
GGA	0.17E–6	0.03E–6	0.92E–6	–0.24E–6	0.0
GGA+U	0.11E–4	0.17E–4	0.58E–3	–0.11E–3	0.0

3.4. DFT optical structuresof Ba_2MWO_6

The optical structures of Ba_2MWO_6 (M = Ni, Zn) have been carried out using LSDA, GGA, LSDA+U and GGA+U methods and shown in Fig. 7 (M = Ni) and Fig. 8 (M = Zn). Direct electronic contributions of the optical dielectric function $\varepsilon(\omega)$, optical conductivity and electron energy-loss function $L(\omega)$ as functions of photon energy are calculated in the energy range 0.0 eV to 40 eV. The $\varepsilon(\omega)$ consists of two main parts, real and imaginary, which can be written as $\varepsilon(\omega)=\varepsilon_1(\omega)+i\varepsilon_2(\omega)$, where $\varepsilon_1(\omega)$ and $\varepsilon_2(\omega)$ represent the real and imaginary parts, respectively. $\varepsilon_1(\omega)$ and $\varepsilon_2(\omega)$ describe the dispersion and dissipation of electromagnetic energy, respectively, and can be obtained from the Kramers–Kronig transformation (KKT) method [29-30]. Moreover, the direct calculation of $\varepsilon_2(\omega)$ is used to evaluate the matrix elements of the electronic dipole operator between the occupied and unoccupied electronic states in valence and conduction bands in any compound. The most significant features of the optical structures are determined by analyzing the electronic structures of Ba_2MWO_6 (M = Ni, Zn). From Figs. 7 and 8, it is clear that the LSDA and GGA spectra are quite similar, as well, the spectra within LSDA+U and GGA+U.

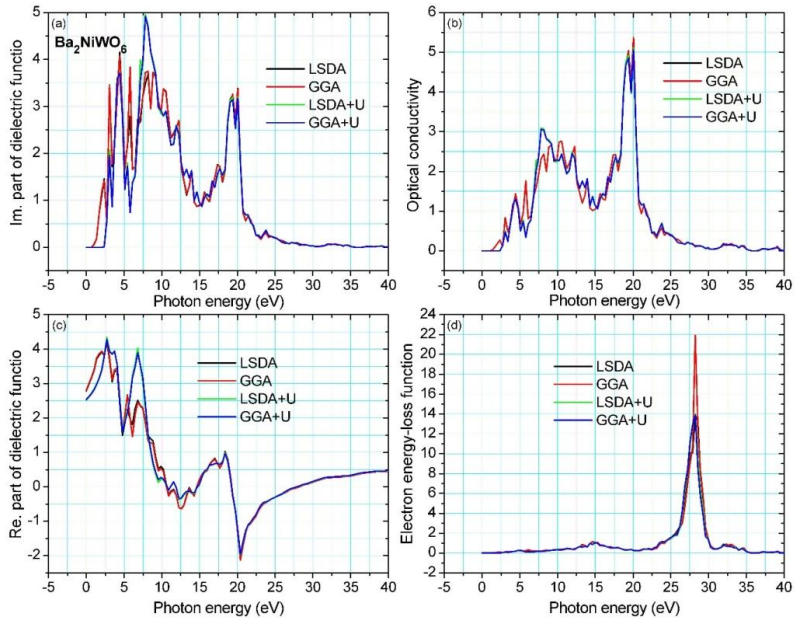

Fig. 7. Optical structures of Ba_2NiWO_6 calculated by LSDA, GGA, LSDA+U and GGA+U methods; (a) imaginary part (Im.) of the dielectric function, (b) optical conductivity, (c) real part (Re.) of dielectric function, and (d) electron loss-energy function.

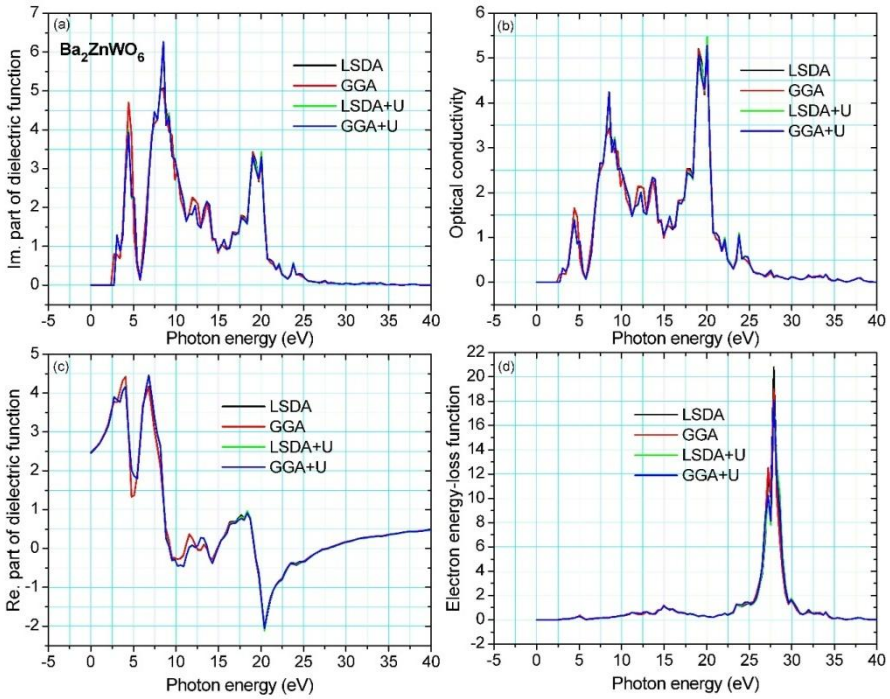

Fig. 8. Optical structures of Ba_2ZnWO_6 calculated by LSDA, GGA, LSDA+U and GGA+U methods; (a) imaginary part (Im.) of the dielectric function, (b) optical conductivity, (c) real part (Re.) of dielectric function, and (d) electron loss-energy function.

The frequency-dependent $\varepsilon_2(\omega)$ is determined by the summation of hops from valence bands to conduction bands. From the $\varepsilon_2(\omega)$ spectra of Ba_2MWO_6 in Figs. 7(a) (M = Ni) and 8(a) (M = Zn), it is seen that they have major optical structures with five sharp peaks range between 2.5 eV and 22.5 eV, and beyond this range, the peaks decrease and reach to zero as the photon energy increases more than 22.5 eV. The positions of these five peaks for (M = Ni) are 3.06 eV, 4.42 eV, 5.78 eV, 8.16 eV and 20.07 eV with $\varepsilon_2(\omega)$ values of 3.45, 4.08, 3.84, 3.75 and 3.37, respectively, from LSDA and GGA, whereas in LSDA+U and GGA+U are 3.06 eV, 4.42 eV, 7.82 eV, 19.05 eV and 20.07 eV with $\varepsilon_2(\omega)$ of 1.96, 3.71, 4.91, 3.14 and 3.20, respectively. For (M = Ni), they positioned at 3.06 eV, 4.42 eV, 8.16 eV, 11.91 eV and 19.05 eV with $\varepsilon_2(\omega)$ values of 0.79, 4.71, 5.01, 2.26 and 3.43, respectively, from LSDA and GGA, while they at 3.06 eV, 4.42 eV, 8.50 eV, 13.61 eV and 20.07 eV with $\varepsilon_2(\omega)$ of 1.29, 4.00, 6.27, 2.16 and 3.43, respectively, in LSDA+U and GGA+U. Therefore, the dielectric spectra of $\varepsilon_2(\omega)$ between 0.0 eV and 2.5 eV are associated with direct band transitions in two compounds. When comparing these spectra with the PDOS of Ba_2MWO_6, Figs 2 and 3, it can be concluded that the direct transitions originate mainly from the hops of the electrons of occupied orbitals in Ni-$3d^8$ and Zn-$3d^{10}$ to the partially unoccupied orbitals in O-$2p^6$, with a tiny effect of W-$5d^0$ orbitals. It is clear from these figures that both compounds have almost same optical spectra. This is attributed to the fact that the characteristics of the conduction bands and the symmetry of wave-functions are somewhat similar, which follow the selection rules and are fully reflected in the matrix of moment elements [31–33]. The calculated conductivity $\sigma(\omega)$ of Ba_2MWO_6 (M = Ni, Zn) are plotted in Figs. 7(b) and 8(b), respectively. It is seen that there is a relationship between $\sigma(\omega)$ and $\varepsilon(\omega)$, which can be represented as $\varepsilon(\omega)=[1+4\pi i\sigma(\omega)]/\omega$ [31]. The electron-dipole transition momentums between the partially occupied and unoccupied states in conduction bands yield major peaks in $\sigma(\omega)$ spectra.

Figs. 7(c) and 8(c) show that the $\varepsilon_1(\omega)$ spectra of Ba_2MWO_6 (M = Ni, Zn) have maximum values between 0.0 eV and 10.0 eV before decreasing to negative values in two ranges, 10.58 eV to 14.79 eV and 19.24 eV to 27.42 eV for (M = Ni); 9.18 eV to 14.97 eV and 19.12 eV to 27.53 eV for (M = Zn). The maximum values of $\varepsilon_1(\omega)$ are 3.87 at 2.40 eV (LSDA) and 2.51 at 6.84 eV (GGA); and 4.33 at 2.64 eV (LSDA+U) and

3.98 at 6.84 eV (GGA+U) for (M = Ni). While for (M = Zn), they are 4.40 at 3.96 eV (LSDA) and 4.14 at 6.77 eV (GGA); and 4.14 at 3.96 eV (LSDA+U) and 4.45 at 6.77 eV (GGA+U). The above results of $\varepsilon(\omega)$ demonstrate that the regions below 0.0 eV exhibit a reflective nature, that is, these regions have a semiconducting feature in two compounds. In addition, when comparing the $\varepsilon_1(\omega)$ spectra with the PDOS of Ba_2MWO_6 in Figs. 3 and 4, it can see that the $\varepsilon_1(\omega)$ spectra have prominent peaks between 1.0 eV and 5.0 eV, which then decreases sharply and pass through zero energy above 10.0 eV, probably due to the strong transitions from the partial valence bands to the unoccupied conduction bands above E_F, more than 2.50 eV in two compounds.The electron loss-energy function (L) describes the energy loss due to the fast electrons itinerant in crystal structures of Ba_2MWO_6 (M = Ni, Zn). Figs. 7(d) and 8(d) show that the L spectra support the obtained results from the $\varepsilon_1(\omega)$ and $\varepsilon_2(\omega)$; there are maximum peaks in two spectra evenly distributed between 25.0 eV and 30.0 eV in both compounds, L = 22 exists at 28.31 eV (LSDA and GGA), and L = 14 exists also at 28.31 eV (LSDA+U and GGA+U) for (M = Ni), whereas for (M = Zn) compound, there is only peak with L = 21.0 at 27.81 eV obtained in all calculations. Also, the L results support the significant electronic configurations of Ni^{2+}-$3d^8$ and Zn^{2+}-$3d^{10}$ in Ba_2MWO_6. Besides, the most intense feature in L spectra of two compounds is the zero peaks (L = 0.0) that appear similarly with a specific width and originated from the elastically scattered electrons.

IV. Conclusion

In this study, the crystal, electronic, magnetic and optical structures of tungstate double-perovskite oxides Ba_2MWO_6 (M = Ni, Zn) were explored using the full potential linear muffin-tin orbital (FP-LMTO) method. The density functional theory (DFT) calculations were carried out by employing the local spin density approximation (LSDA) and generalized gradient approximation (GGA). Also, the effect of exchange-correlation energies (U and J) on M-3d and W-5d states were considered in LSDA+U and GGA+U calculations. Both double perovskites Ba_2MWO_6 (M = Ni, Zn) show an ordered structure with a face-centered cubic symmetry and space group $Fm\bar{3}m$, where the structures contain alternating MO_6 and WO_6octahedra that almost fully ordered in the crystal space. All LSDA, LSDA+U, GGA and GGA+U calculations accurately depicted the semiconducting and antiferromagnetic (AF) ground states in two compounds with small differences in energy gaps and partial spin magnetic moments. The calculated total and partial density of states showed that the Ba_2MWO_6 compounds contain semiconducting energy gaps in spin-up and spin-down channels, and it is found that the M-site replacement and U energy, in LSDA+U and GGA+U, are responsible for the small difference in energy-gap values. Also, it is established that the electronic and magnetic structures of Ba_2MWO_6 are produced due to the AF indirect long-range coupling M^{2+}-$3d^n_{\uparrow}$–O^{2-}-$2p^6$–W^{6+}-$5d^0_{\downarrow}$, with n = 8 for (M = Ni) and n= 10 for (M = Ni). In addition, the optical structures of Ba_2MWO_6 (M = Ni, Zn) were investigated in detail. The real and imaginary parts of the dielectric function, optical conductivity, and electron energy-loss function were calculated and their main features were analyzed.

References

[1]. K.-I. Kobayashi, T. Kimura, H. Sawada, K. Terakura, Y. Tokura, Nature 395, (1998), 677–680.
[2]. Horng-TayJeng, G. Y. Guo, Phys. Rev. B 67, (2003), 094438.
[3]. W. Zhong, W. Liu, C.T. Au, Y.W. Du, Nanotechnology 17, (2006), 250.
[4]. T.S. Chan, R.S. Liu, G.Y. Guo, S.F. Hu, J.G. Lin, J.-F. Lee, L.-Y. Jang, C.-R. Chang, C.Y. Huang, Solid State Commun. 131(8), (2004), 531.
[5]. D.P. Rai, A. Shankar, M.P. Ghimire, Sandeep, R.K. Thapa, Comput. Mater. Sci. 101, (2015), 313–320.
[6]. S.A. Ivanov, S.-G. Eriksson, R. Tellgren, H. Rundlöf, M. Tseggai, Mater. Res. Bull. 40(5), (2005), 840–849.
[7]. A. FakhimLamrani, M. Ouchri, A. Benyoussef, M. Belaiche, M. Loulidi, J. Magn. Magn. Mater. 345, (2013), 195–200.
[8]. M. Musa Saad H.-E., N. Rammeh, Physica B 481, (2016), 217–223.
[9]. A.K. Azad, S.A. Ivanov, S.-G. Eriksson, J. Eriksen, H. Rundlöf, R. Mathieu, P. Svedlindh, Mater. Res. Bull. 36, (2001), 2215–2228.
[10]. YoshieiTodate, WataruHigemoto, KusuoNishiyama, KazumaHirot, J. Phys. Chem. Solids 68, (2007), 2107–2110.
[11]. C.A. López, M.E. Saleta, J. Curiale, R.D. Sánchez, Mater. Res. Bull. 47(5), (2012), 1158–1163.
[12]. D.D. Khalyavin, Jiaping Han, A.M.R Senos, P.Q. Mantas, J. Mater. Res. 18(11), (2003), 2600–2607.
[13]. Fei Zhao, Zhenxing Yue, ZhilunGui, Longtu Li, Jpn. J. Appl. Phys. 44, 11, (2005), 8066.
[14]. Guo San-Dong, Chinese Physics B 22(6), (2013), 067102.
[15]. U. von Barth, L. Hedin, J. Phys. C: Solid State Phys. 5, (1972), 1629.
[16]. John P. Perdew, Yue Wang, Phys. Rev. B 45, (1992), 13244–13249.
[17]. Jing Wang, Jian Meng, Zhijian Wu, Chem. Phys. Lett. 501, 4–6, (2011), 324–329.
[18]. M. Musa Saad H.-E., Comput. Mater. Sci. 111, (2016), 481–488.
[19]. Daniel Stoeffler,Corina Etz, J. Phys.: Conden. Matter 18 (49), (2006), 1129–11300.
[20]. S. Yu. Savrasov, D. Yu. Savrasov, Phys. Rev. B 46, (1992), 12181–12195.
[21]. S.Y. Savrasov, "FULL-POTENTIAL PROGRAM PACKAGE"LMTART 6.50" USER's MANUAL", New Jersey Institute of Technology, May 2, (2004).
[22]. Shannon, ActaCryst. A32, (1976), 751–767.
[23]. M.W. Lufaso, P. M. Woodward, Acta. Crystallogr., Sec. B 57, (2001), 725.

[24]. BouchaibManoun, A. Ezzahi, S. Benmokhtar, L. Bih, Y. Tamraoui, R. Haloui, F. Mirinioui, S. Addakiri, J.M. Igartua, P. Lazor, J. Mol. Struct. 1045, (2013).
[25]. Yousif A. Alsabah, Mohamed A. AlSalhi, Abdelrahman A. Elbadawi, Eltayeb M. Mustafa, J. Alloys Compd. 701, (2017), 797–805.
[26]. Shaveen Garg, M.M. Sinha, H.C. Gupta, Physica B 433, (2014), 107–111.
[27]. O. Sahnoun, H. Bouhani-Benziane, M. Sahnoun, M. Driz, C. Daul, Comput. Mater. Sci. 77 (2013) 316–321.
[28]. Daniel E. Bugaris, Jason P. Hodges, AshfiaHuq, Hans-Conrad zurLoye, J. Solid State Chem. 184, (2011), 2293–2298.
[29]. F. Wooten, Optical Properties of Solids, Academic Press, New York (1972).
[30]. M. Fox, Optical Properties of Solids, Oxford University Press, Oxford (2011).
[31]. Wilayat Khan, A.H. Reshak, J. Mater Sci. 49, (2014), 1179–1192
[32]. Iftikhar Ahmad, B. Amin, M. Maqbool, S. Muhammad, G. Murtaza, S. Ali, N.A. Noor, Chin. Phys. Lett. 29, (2012), 097102.
[33]. B. Amin, I. Ahmad, M. Maqbool, S. Goumrisaid, R. Ahmad, J. Appl. Phys. 109, (2011), 023109.

IOSR Journal of Applied Physics (IOSR-JAP) is UGC approved Journal with Sl. No. 5010, Journal no. 49054.

M. Musa Saad H.-E " Crystal, electronic, magnetic and optical structures of cubic double perovskites Ba2MWO6 (M = Ni, Zn)." IOSR Journal of Applied Physics (IOSR-JAP) , vol. 11, no. 6, 2019, pp. 41-52.